2014

University of Genoa - DICCA

Prof : Jan Oscar Pralits

Lab Assistant : Matteo Colli

Student : Stefano Pastorino

[ADVANCED FLUID DYNAMICS]

Effects of flap deflection on airfoil performance at a low Reynolds number: optimization for NACA 0012

1. Introduction

The analysis of the two dimensional subsonic flow over a NACA 0012 airfoil using OpenFoam is presented. This work has been realized following an accurate sequence of steps: first of all, the geometry and the flap have been created. Then, it has been important to launch various simulations by altering only the angle of attack from 0° to +20° with steps of 5° so as to find the angle that causes an evident flow separation and a high value of the drag coefficient. In consequence of this result, the aim of this work is to show the behavior of the airfoil, with the latter angle of attack, by varying the flap position from -9° to +15° in order to optimize it and minimize the drag coefficient of the airfoil. All these simulations have been run for a low Reynolds number (500), in fact they constitute the first part of a broader framework in which calculations will be also evaluated for higher Reynolds numbers.

2. Problem formulation

Simulations have been performed using the Navier-Stokes equations[1]. The derivation of the Navier-Stokes equations begins with an application of Newton's second law: conservation of momentum (often alongside mass and energy conservation) being written for an arbitrary portion of the fluid. In an inertial frame of reference, the general form of the equations of fluid motion is:

$$\begin{cases} \rho\left(\frac{\partial v}{\partial t}+v\cdot\nabla v\right)=-\nabla p+\nabla\cdot T+f \\ \frac{\partial \rho}{\partial t}+\nabla\cdot(\rho v)=0 \end{cases} \tag{2.1}$$

where

- v is the flow velocity,
- ρ is the fluid density,
- p is the pressure,
- T is the (deviatoric) component of the total stress tensor, which has order two,
- f represents body forces (per unit volume) acting on the fluid

In our case, the solver is applied to simulate the incompressible flow around the NACA 0012 airfoil considering constant viscosity, so the N-S equations are simplified:

$$\begin{cases} \rho\left(\frac{\partial v}{\partial t}+v\cdot\nabla v\right)=-\nabla p+\mu\nabla^2 v+f \\ \nabla\cdot v=0 \end{cases} \tag{2.2}$$

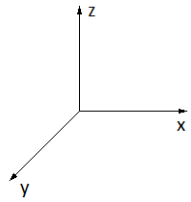

where x is the streamwise direction, y is the direction of the depth axis and z is the direction long the vertical axis.
The fluid domain is represented by a rectangle containing the airfoil with an x side of 22m and a z side of 12m:

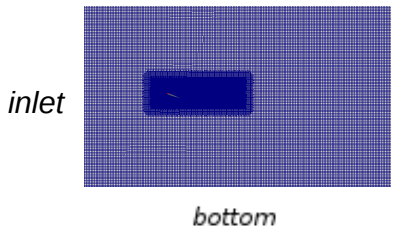

Fig. 2.1
fluid domain

In terms of initial conditions, it's important to refer to pressure and velocity: pressure initial condition is uniform in the internal field and equal to zero value, instead the initial velocity field is uniform but not zero value in the direction of motion where $v = 0{,}005\ ^{m}/_{s}$.

In regard to boundary conditions, the fluid domain presents null normal gradient of pressure for inlet, top and bottom and null normal velocity components for top and bottom.
As for the line of the airfoil, normal gradient of pressure is zero and velocity components are zero.

3. Optimization

In this chapter the main step of the work is presented. As previously said, the purpose of this project is to study how the drag coefficient of the airfoil can be minimized by moving the flap. So the optimization of the problem is reduced to one parameter: the flap position. This fact allows a streamlined process by using a handmade optimization; indeed a new geometry has been created for each flap position and simulated from -9° to +15° as shown in Fig. 3.1.

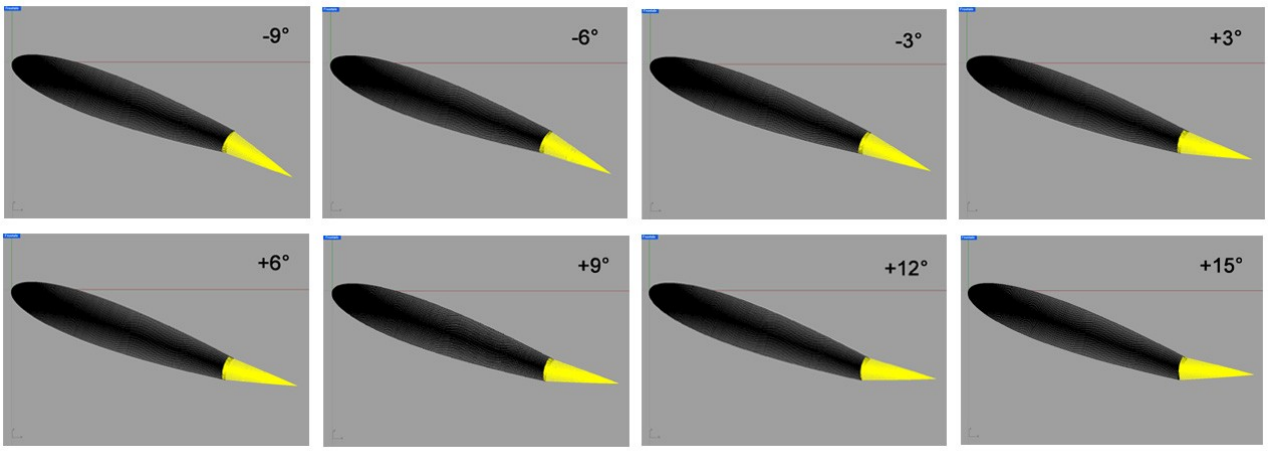

Fig. 3.1 airfoil with different flap positions

In another way, optimization could have been done automatically by using one of the gradient methods like Steepest Descent[2]. The latter method is based on the observation that if the multivariable function $F(x)$ is defined and differentiable in a neighborhood of a point a, then $F(x)$ decreases fastest if one goes from a in the direction of the negative gradient of F at a, $-\nabla F(a)$. It follows that, if $b=a-\delta\nabla F(a)$ for δ small enough, then $F(a)\geq F(b)$.

Fig. 3.2 approaching to the minimum

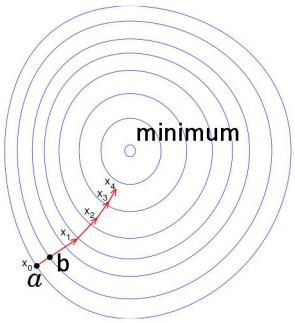

With this observation in mind, one starts with a guess x_0 for a local minimum of F and considers the sequence $x_0, x_1, x_2, \ldots$ such that $x_{n+1}=x_n-\delta_n\nabla F(x_n), \quad n\geq 0$.

We have $F(x_0)\geq F(x_1)\geq F(x_2)\geq \ldots$, so hopefully the sequence (x_n) converges to the desired local minimum. In our case the iterative procedure should be:

$$\beta_{n+1}=\beta_n-\delta_n\left(\frac{\partial C_D}{\partial \beta}\right)_n \qquad (3.1)$$

where

β_n is the n-th angle of the flap

δ_n is the step length of the n iteration

C_D is the drag coefficient

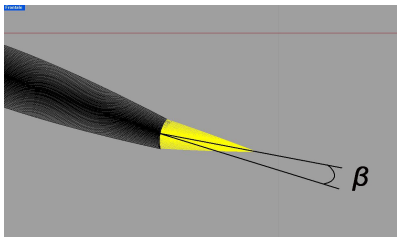

Fig. 3.3 angle β

4. Problem resolution

The OpenFOAM® CFD Toolbox[3] is an open source CFD software package which has a large user base across most areas of engineering and science, from both commercial and academic organizations. An extensive set of OpenFOAM solvers has evolved (and is forever growing) that are available to users. In particular, in this work icoFoam has been selected; icoFoam solves the incompressible laminar Navier-Stokes equations using the PISO algorithm.

The computational domain of this work is composed of about 55000 cells emerged in a structured way, taking care of the refinement of the grid near the airfoil in such a way as to enclose the boundary layer approach. Calculations are done for constant air velocity, evaluated in order to have a low Reynolds number (500).

4.1 Geometry creation

The NACA 0012 airfoil has been chosen as geometry for its symmetry which makes it suitable for an easier but reliable analysis. First of all, the surface of the airfoil has been created starting from the profile coordinates using a CAD Software named Rhinoceros; then, the surface has been extruded in y direction from -1 to 1 (as shown in Fig. 4.1.1a) because OpenFoam needs a 3D mesh although the problem is 2D. Finally, the solid has been converted in a polygon mesh and saved as a stl file.

As regards the flap, it has been designed conventionally: its length is 20% of the chord as shown in Fig. 4.1.1b .

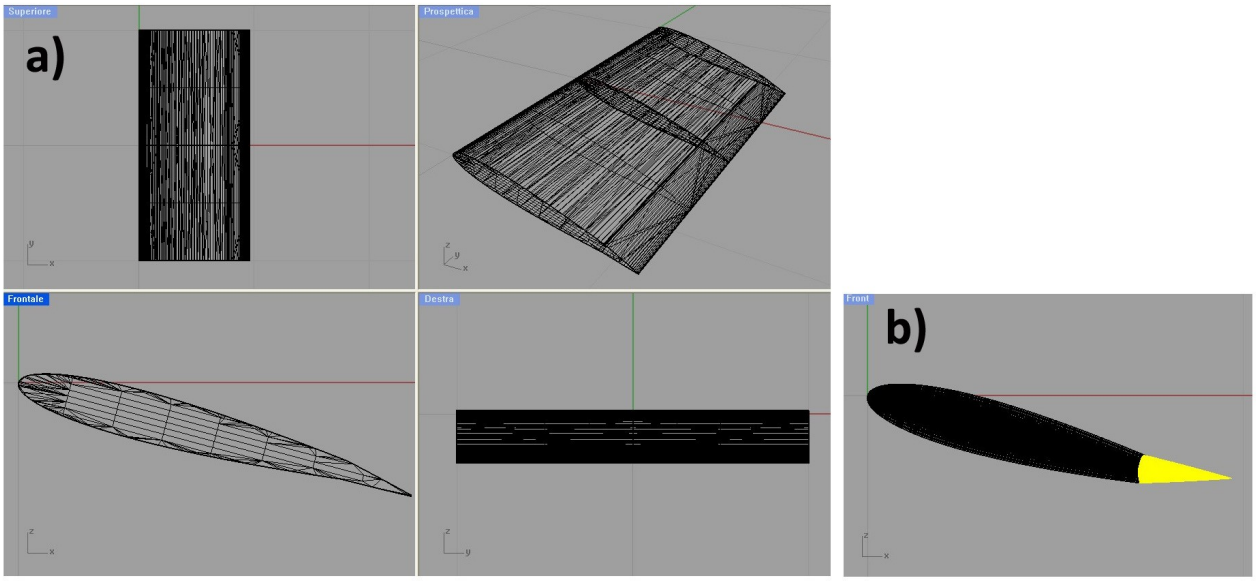

Fig. 4.1.1 : a) surface extruded on the left ; b) flap representation on the right

4.2 Mesh and Grid generation

One of the most essential step of this work is the mesh and grid generation. After importing the geometry in OpenFoam, it's important to customise the grid around it appropriately. For this purpose, OpenFoam provides the right tools: blockMesh and SnappyHexMesh.

SnappyHexMesh is a mesh generation utility for 3-dimensional meshes containing hexahedra and split-hexahedra automatically from triangulated surface geometries in Stereolithography format. The mesh approximately conforms to the surface by iteratively refining a starting mesh and morphing the resulting split-hex mesh to the surface. The specification of mesh refinement level is very flexible and the surface handling is robust with a pre-specified final mesh quality.

Before snappyHexMesh is executed a background mesh of hexahedral cells (that fills the entire region within) must be created (Fig. 4.2.1); this has been done using BlockMesh.

In Fig. 4.2.1 the first and the second mesh refinement region are also shown (particular), instead the last three are shown in Fig. 4.2.2

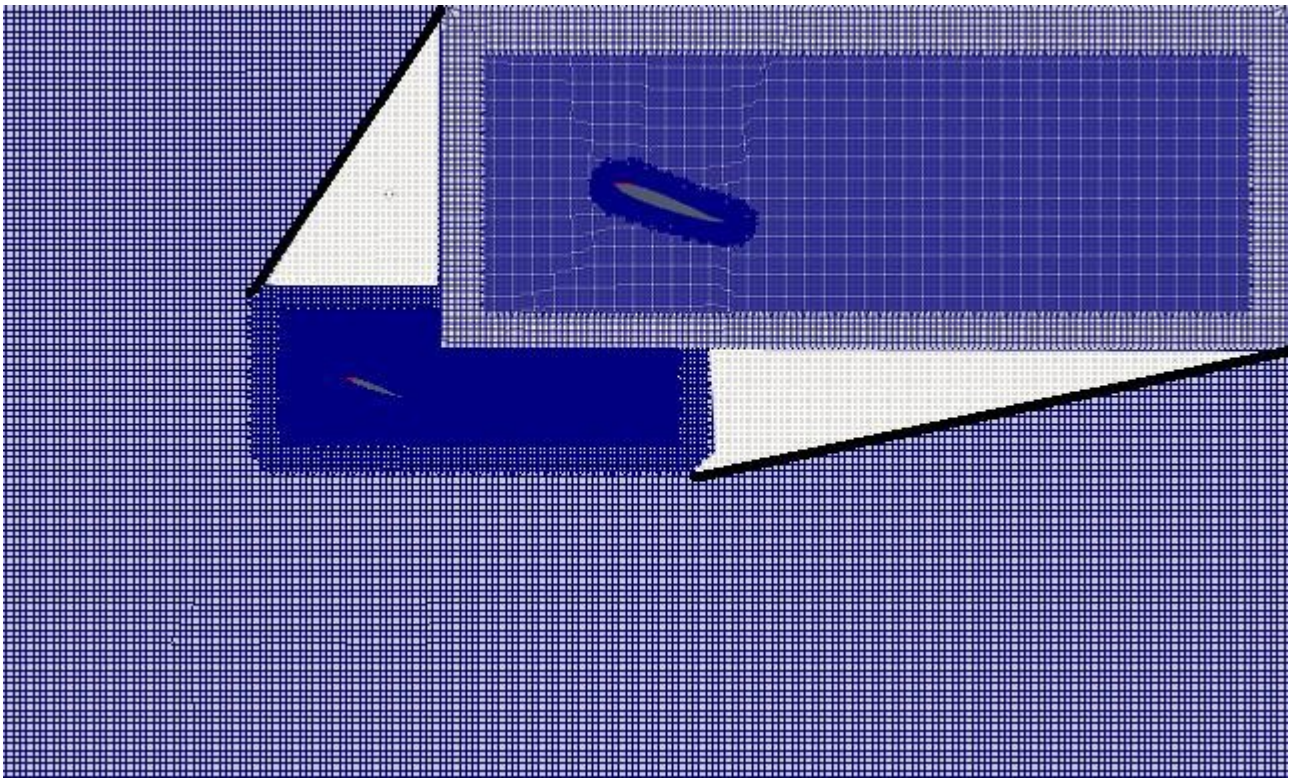

Fig 4.2.1 domain: the grid created using BlockMesh and the particular of the mesh refinements

After these refinements, cells have been selected for splitting in the locality of a specified surface and then a process of cell removal has started.

Cell removal requires one or more regions enclosed entirely by a bounding surface (in our case the airfoil) within the domain; cells are retained if 50% or more of their volume lies within the region. The remaining cells have been removed accordingly as illustrated in Fig. 4.2.2 a): this is the first refinement level.

The next stage of the meshing process (second refinement level) has involved moving cell vertex points onto surface geometry to remove the jagged surface from the mesh as shown in Fig 4.2.2 b). The surface snapping can produce some irregular cells along the boundary surface, so the third refinement level has been used.

Thanks to the last step, additional layers of hexahedral cells aligned to the boundary surface have been introduced as illustrated in Fig. 4.2.2 c).

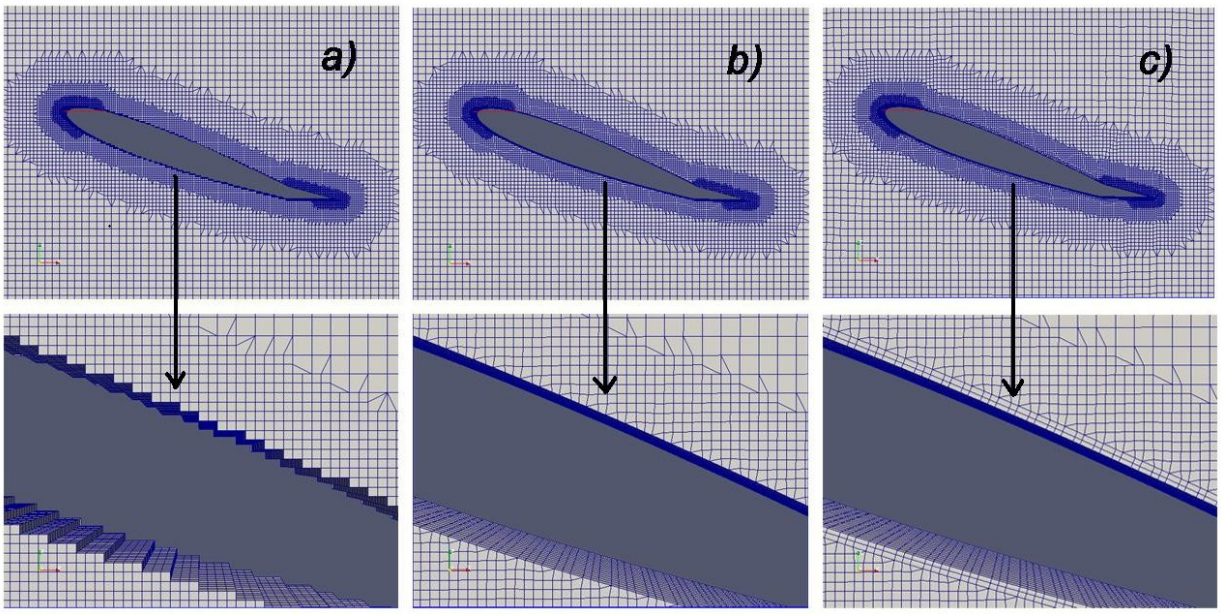

Fig. 4.2.2 refinement levels and respective underlying particulars

5. Results

Numerical simulations always need a grid convergence study in order to find the optimal cell size. The goal is to obtain Δx and Δz (cell dimensions respectively in x and z direction, Fig 5.1) such that force coefficients don't change if these lenghts decrease; that is why, before the beginning of the official simulations, a set of them have been launched by varying the number of cells of the principal grid in x and z direction, instead grid dimensions remained the same.

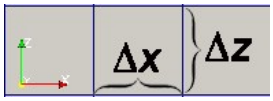

Fig. 5.1 cell dimensions

The optimal number of cells has been 220 in x direction (along the side of 22) and 120 in z direction (along the side of 12) in fact, as shown in the following table,

the increase of cells doesn't really modify the force coefficients:

Angle of attack	Number of cells	C_D	C_l
0°	(220; 120; 1)	2.1973e-01	-6.46e-05
0°	(230; 130; 1)	2.1977e-01	-5.35e-05

Tab. 5.1 variation of cell size

Therefore it's important to consider the numerical stability of the problem through the Courant number. The Courant condition[4] is necessary for stability while solving certain partial differential equations numerically by the method of finite differences; it arises in the numerical analysis of explicit time integration schemes, when these are used for the numerical solution.

As a consequence, time step must be less than a certain value in many explicit time-marching computer simulations, otherwise the simulation will produce incorrect results.

For the two-dimensional case, the Courant condition has the following form:

$$Co = u_x \frac{\Delta t}{\Delta x} + u_z \frac{\Delta t}{\Delta z} \leq Co_{max} \tag{5.1}$$

where

Δt is the time step size

Δx and Δz are the dimensions of the grid cell at each location

u_x and u_z are the average linear velocities at that location respectively in x and z direction

In our case, the (low) velocity field develops especially in x direction, so the relation 5.1 can be simplified as follows:

$$Co = u_x \frac{\Delta t}{\Delta x} \leq 1 \tag{5.2}$$

A physical explanation, for a CFD simulation, of the Courant number could be that it tells you something about how fluid is moving through your computational cells. Meaning that If the Courant number is <= 1 , then the fluid particles move from one cell to another within one time step (at most). While if the Courant number is >1 a fluid particle move through two or more cells at each time step and this can affect negatively the convergence.

In this work, the Co_{max} has been monitored in order to not exceed the limit of 0.3 (as usually when the solver is icoFoam), while the time step size has been 0.1s with a total simulation of 3600s.

5.1 Research of the critical angle of attack

Before optimizing the flap position computations have been performed in order to find the angle of attack that causes the flow separation as shown in Fig 5.1.1 and 5.1.2 .

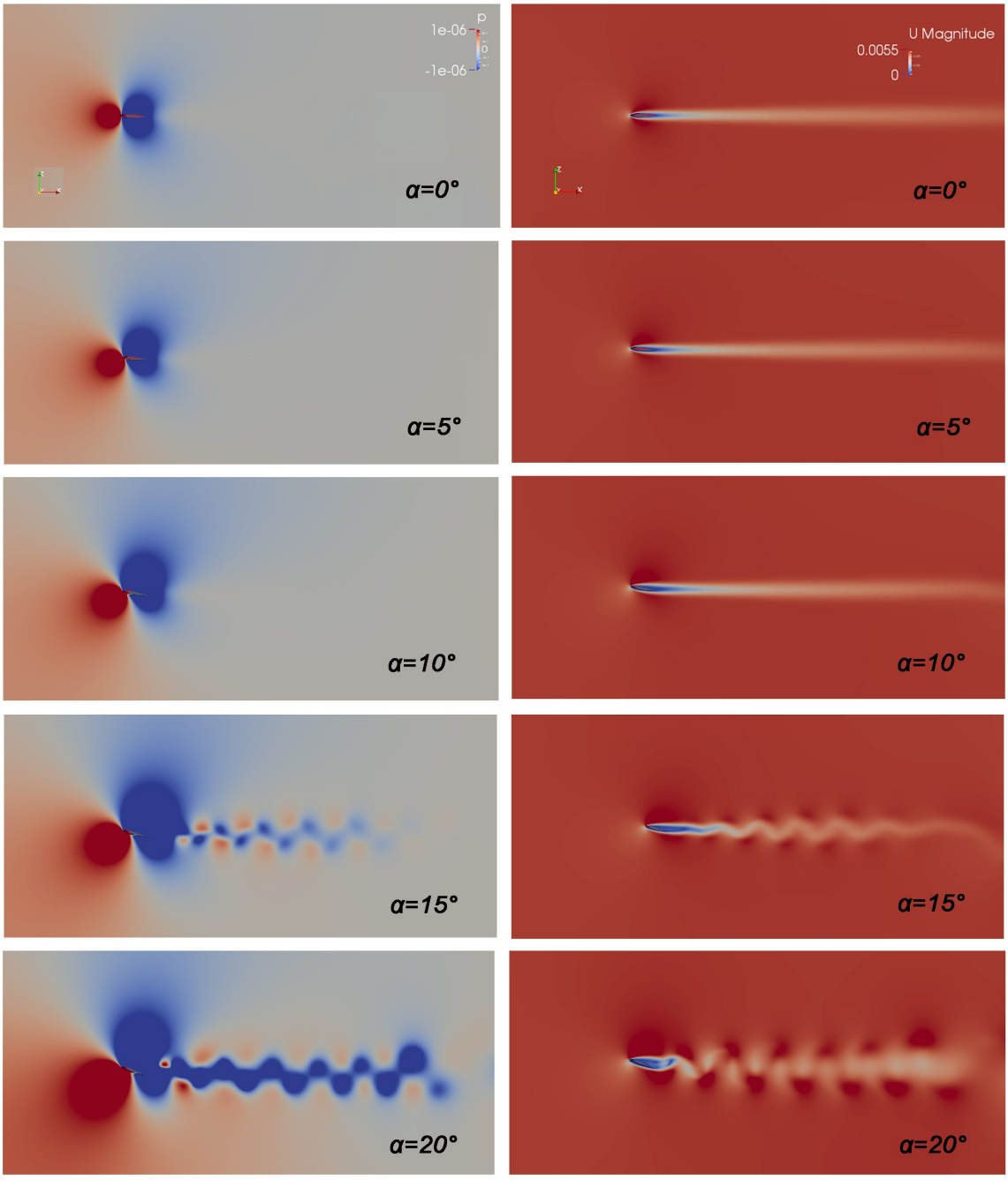

Fig. 5.1.1 foot prints of pressure (on the left) and velocity (on the right) for different angles of attack

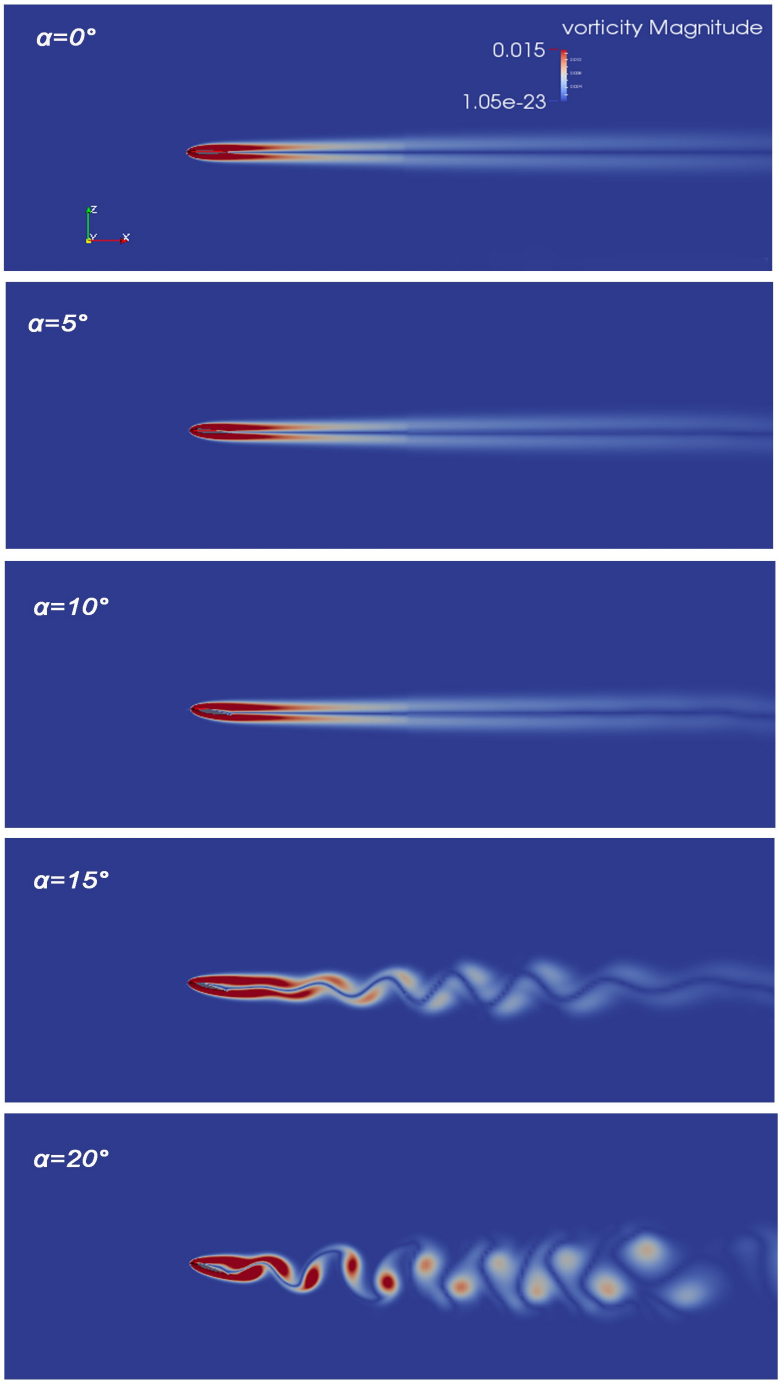

Fig. 5.1.2 foot prints of vorticity

Flow separation starts between α=+10° and α=+15° and it grows till α=+20°: as can be seen in Fig. 5.1.2, Von Karman vortex street starts at α=+15°, but the critical angle for which Von Karman vortex street is well rendered is α=+20°. That is why the rest of the work has been conducted in order to minimize the drag coefficient of the airfoil with this setting, that results the highest value: $C_D(20°) = 0.42$ (Fig. 5.1.3)

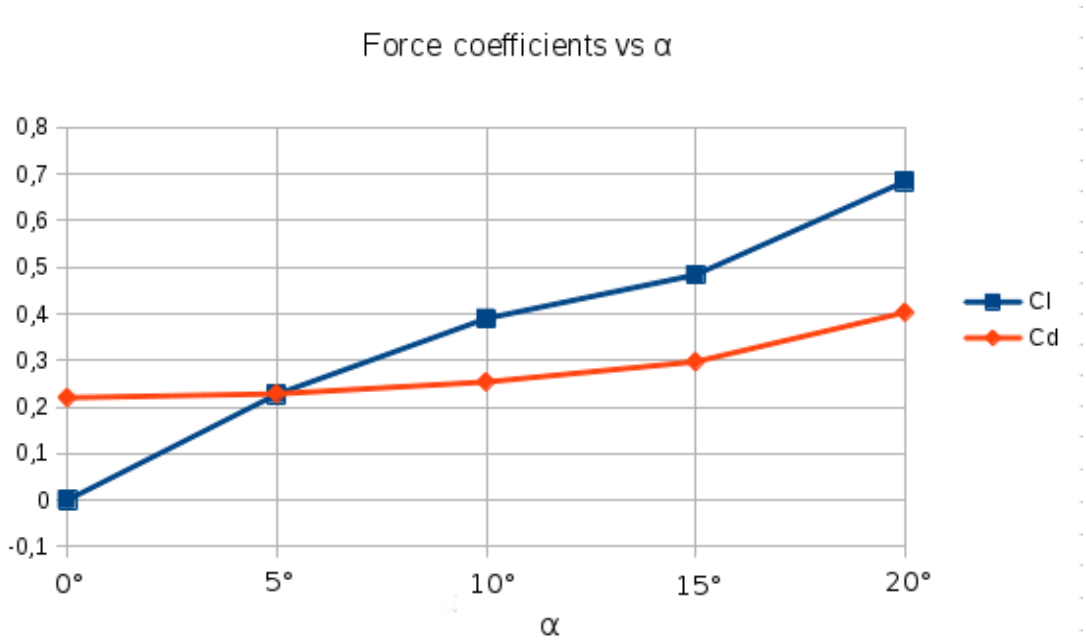

Fig. 5.1.3 Force coefficients vs angle of attack

The graphic in Fig. 5.1.3 shows us the lift and drag coefficients varying the angle of attack; the values from 0° to 15° are instantaneous values (C_l and C_D solutions are constant in time), instead the value at 20° is a mean value because C_l and C_D are oscillatory solutions for all the simulated time.

5.2 Varying the flap position

Now let's change over to the last step of the work: the airfoil analysis results by varying the flap position is presented.
As previously mentioned, the flap position has been varied from -9° to +15° with step of 3° in order to have a substancial and reliable range to analyze.

As shown for the cases represented in Fig. 5.2.1 , the flap doesn't avoid flow separation, but vorticity decreases from -9° to +15° slowly. This latter event can be deduced by analyzing the vorticity magnitude for each vortex street in Fig. 5.2.1 , in fact the vortex street tends to dissolve itself by increasing the angle of the flap.

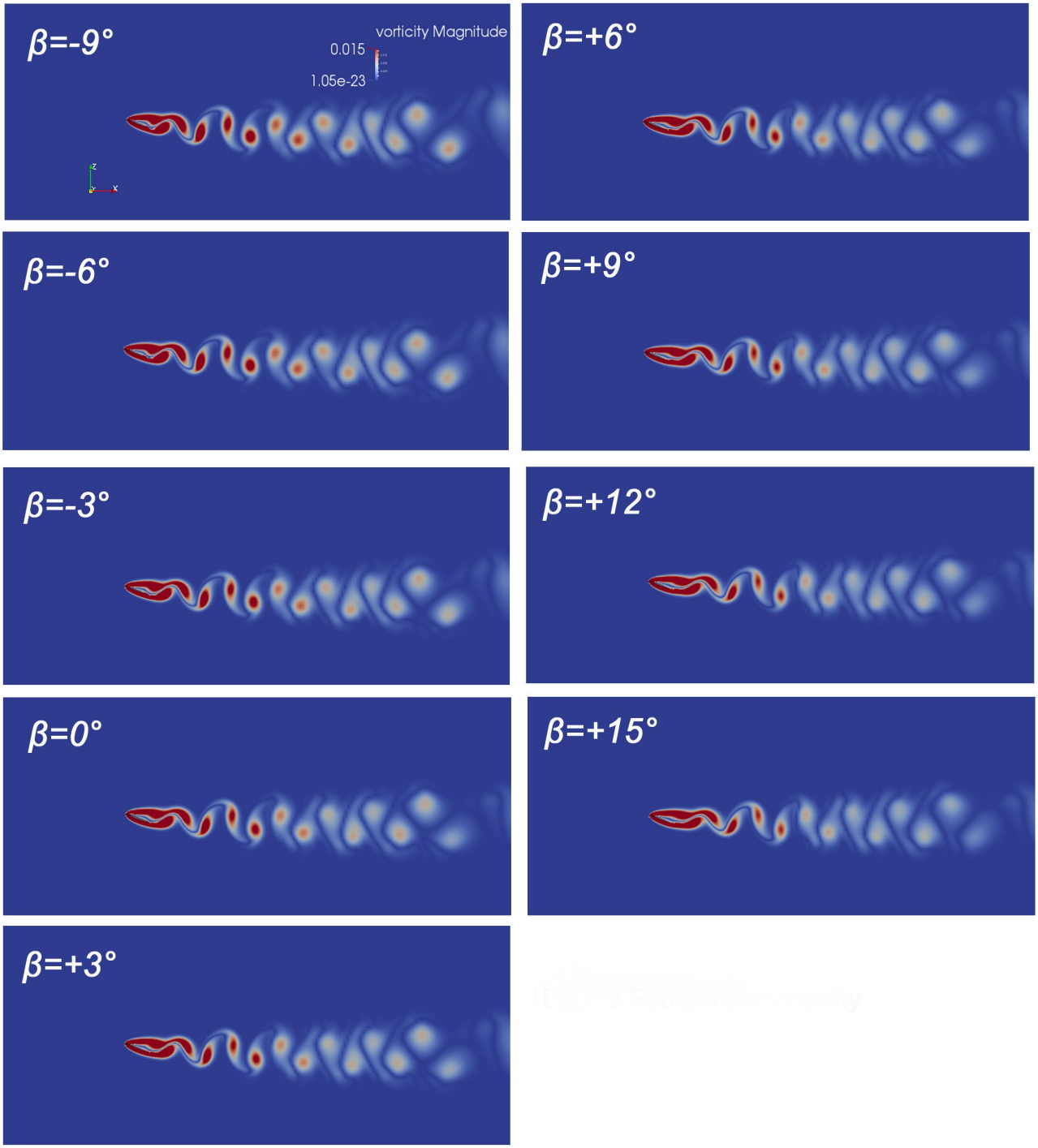

Fig. 5.2.1 Footprint of vorticity by varying β

The flap's effect clearly emerges from plots below. It stands to reason that C_L and C_D have similar trend (Fig. 5.2.2 and Fig. 5.2.3) because the extension of the flap from 0° to negative values of β causes an enlargement of the airfoil surface that deflects more volume of fluid; it means that lift increases, but drag increases too. On the other hand, lift and drag decrease by moving toward positive angle of the flap and this is what we have to look for. The decrease of C_D directly depends on the reduction of the region of separated flow; in fact, as we can see in Fig. 5.2.1 , the red region around the airfoil, which represents the area with the highest vorticity magnitude, tails off from -9° to +15° reducing losses and drag.

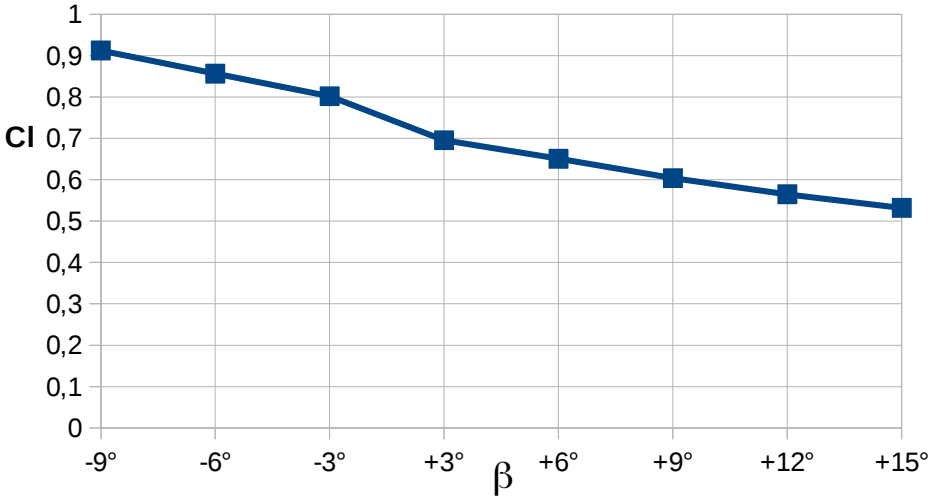

Fig. 5.2.2 lift coefficiet vs the angle of the flap

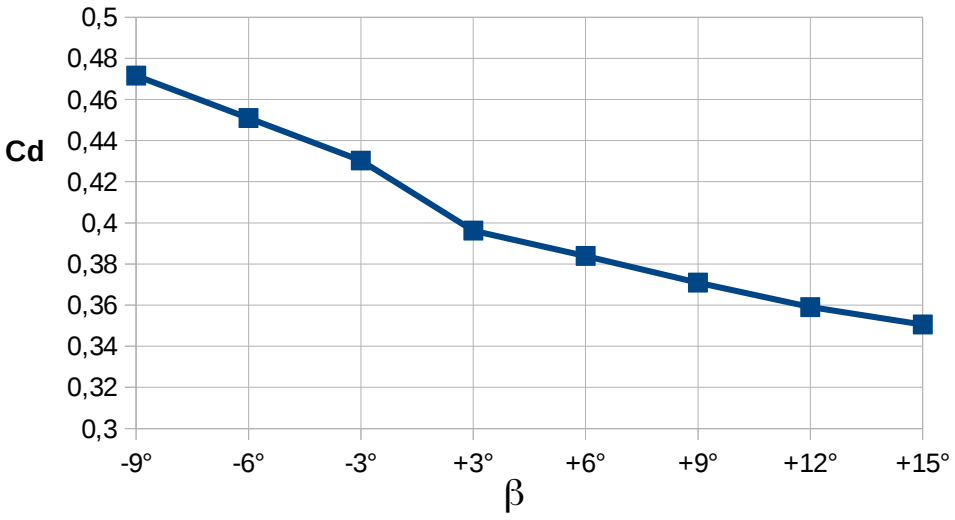

Fig. 5.2.3 drag coefficient vs the angle of the flap

As shown by Fig. 5.2.2 and 5.2.3 $C_L > C_D$ for all the flap positions simulated, however a new fact comes to light from the following figure: the lift coefficient decreases more quickly than the drag coefficient in the same range (from -9° to +15°). This is caused by the presence of the separated region that decreases, yet it makes it slowly provoking the same slow reduction for C_D .

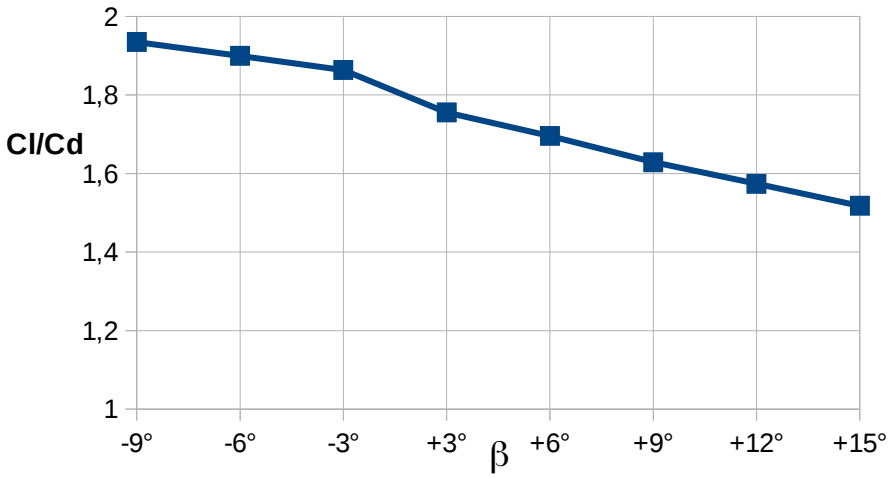

Fig. 5.2.4 relation between the two force coefficients by varying β

In the end, for what concerns the pitch moment coefficient, it is easy to see that simulations give a negative C_m ; it means that the airfoil tends to get lower the leading edge because the barycenter is more advanced than the point of application of the lift.

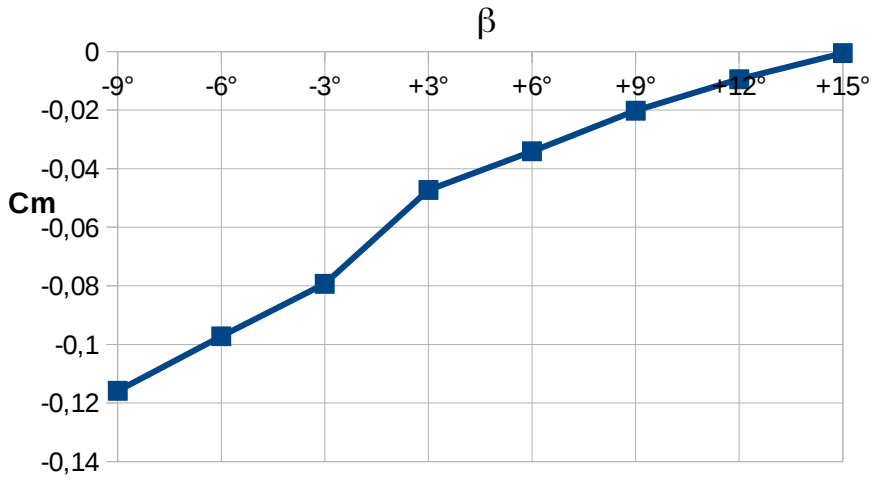

Fig. 5.2.5 pitch moment coefficient vs the angle of the flap

All the points represented in the four graphics above are average values over time because C_l, C_D and C_m are oscillatory solutions.

In conclusion, it's possible to affirm that the goal of this work has been achieved, especially the optimal flap position that minimize the drag coefficient of the airfoil (for α =20°) has been found: β = +15°. However, the trend of C_D has been such interesting that more simulations have been launched for higher angles of the flap: in particular the new aim of the work has been the search for a minimum value for C_D and C_L joined to the the analysis of the footprint of vorticity.

5.3 Higher angles of flap

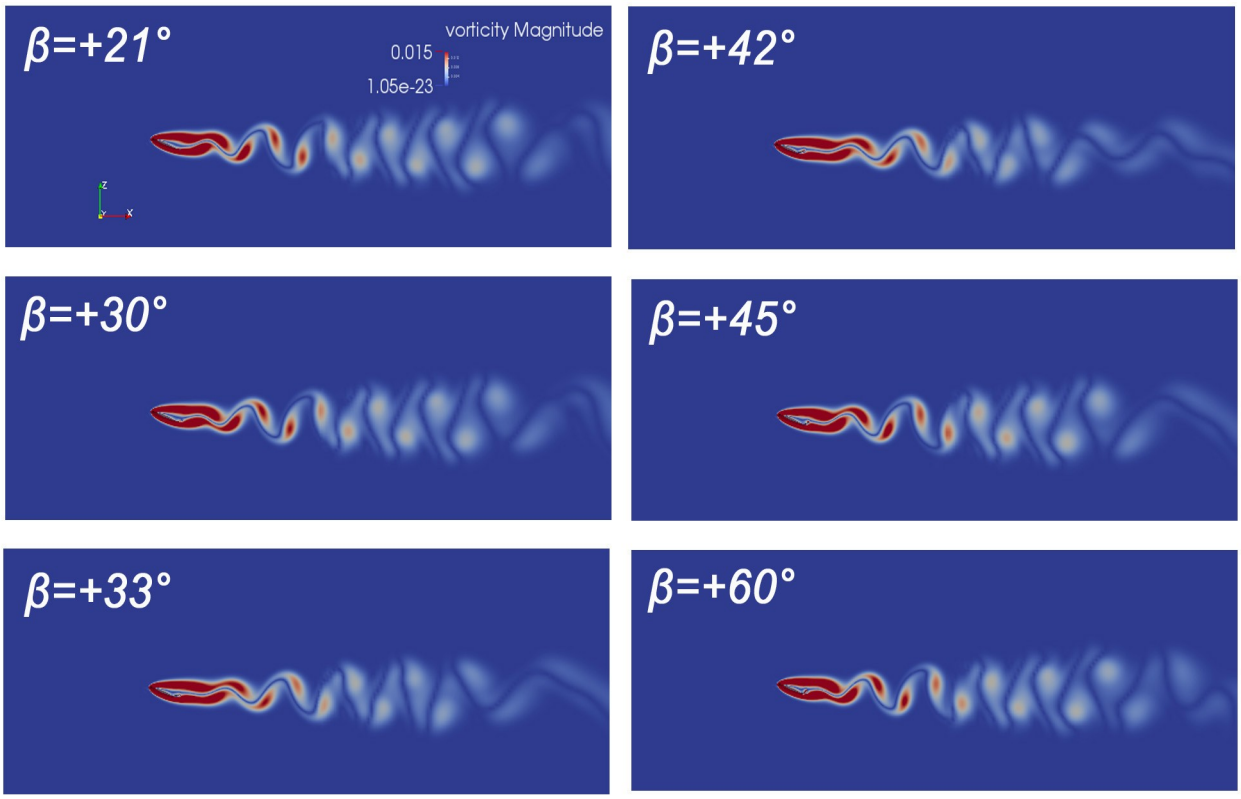

Fig. 5.3.1 Footprint of vorticity

The Fig. 5.3.1 shows the footprint of vorticity for high angles of flap; as can be seen, vorticity magnitude decreases until β = +42° for which the vortex street seems to dissolve itself. After this value vorticity magnitude gradually grows until the last flap position simulated that is β = +60°.

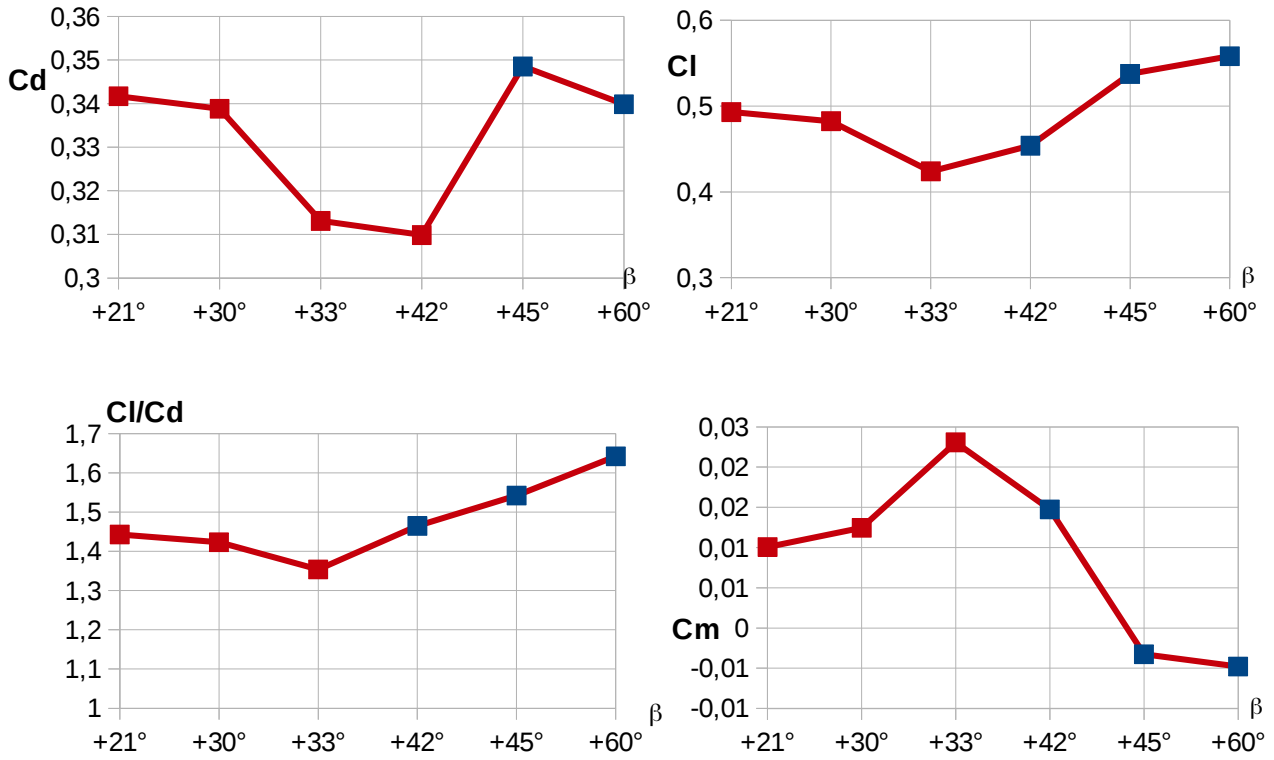

Fig. 5.3.2 force and momentum coefficients vs β

The first part (red points) of each trend represented in Fig. 5.3.2 is similar to the respective trend for low angles of flap (chapter 5.2), instead the second part (blue points) is conditioned by a new flow separation on the flap.

In fact, it is clearly evident that C_D and C_L continue to decrease from +15° to +42° for C_D and from +15° to +33° for C_L ; the trend of C_D is joined to the vorticity magnitude (Fig. 5.3.1) in fact, after β = +42° C_D grows by following the increase of vorticity. For the same reason the relation C_L / C_D inverts his trend from +33°.

The pitch moment coefficient confirms this growing trend from +21° to +33° yet it changes sign to positive values, which means that the airfoil tends to raise the leading edge because the barycenter is less advanced than the point of application of the lift. After β = +33° C_m decreases until it becomes negative again.

6. Conclusions

This work consists of two parts: the first one is the search for the optimal flap position from -9° to +15° in order to minimize the highest value of the drag coefficient found for α=+20°:

$C_D(+20°)_{\beta=0°}=0.42$ is reduced to $C_D(+20°)_{\beta=+15°}=0.35$

The second part is the natural extension of the first, in fact simulations continue for higher angles of flap in order to search for the minimum value of C_D ; as consequence:

$C_{Dmin}(+20°)=C_D(+20°)_{\beta=42°}=0.31$

β is the angle of the flap

α is the angle of attack

Next steps:

- calculations will be evaluated for higher Reynolds numbers.
- a new work based on the study about the creation and the growth of the region of separeted flow on the flap for high values of β will be realized.

References

[1] Computational Fluid Dynamics – John F. Wendt (Ed.)
With Contributions by John D. Anderson Jr., Joris Degroote, Gerard Degrez, Erik Dick, Roger Grundmann and Jan Vierendeels

[2] The Steepest Descent Method – Springer US (Ed.)
Michael Bartholomew-Biggs

[3] OpenFOAM - the open source CFD toolbox
http://www.openfoam.com/

[4] CFD Online
http://www.cfd-online.com/